Model	$T_{\rm eff}$ log$g$	Depth	Boundary of instability	$z(v_{\rm rms}=$ 100 m/s)	Bottom of model	Velocity Scale Height	
AT85g41N3	8500 K	z [km]	-12900	-16730	-17920	$H_{\rm v}$ [km]	1284
	4.13	P [dyn/cm^2]	0.84*10^6	1.68*10^6	2.03*10^6	$H_{\rm v}$ [H$_{\rm p}$]	0.219
		$\Delta M[10^{-9}M_*]$	3.87	7.74	9.35		
AT85g44N1	8500 K	z [km]	-6800	-9120	-10120	$H_{\rm v}$ [km]	741
	4.40	P [dyn/cm^2]	1.14*10^6	2.47*10^6	3.30*10^6	$H_{\rm v}$ [H$_{\rm p}$]	0.231
		$\Delta M[10^{-9}M_*]$	1.51	3.28	4.39		
AT85g44N2	8500 K	z [km]	-6800	-8600	-12670	$H_{\rm v}$ [km]	781
	4.40	P [dyn/cm^2]	1.14*10^6	2.11*10^6	6.47*10^6	$H_{\rm v}$ [H$_{\rm p}$]	0.227
		$\Delta M[10^{-9}M_*]$	1.51	2.80	8.60		
AT85g44N8	8500 K	z [km]	-6920	-9070	-12670	$H_{\rm v}$ [km]	975
	4.40	P [dyn/cm^2]	1.2*10^6	2.41*10^6	6.47*10^6	$H_{\rm v}$ [H$_{\rm p}$]	0.284
		$\Delta M[10^{-9}M_*]$	1.59	3.20	8.60		
AT85g44N01	8500 K	z [km]	-6920	-9050	-12670	$H_{\rm v}$ [km]	987
	4.40	P [dyn/cm^2]	1.2*10^6	2.40*10^6	6.47*10^6	$H_{\rm v}$ [H$_{\rm p}$]	0.287
		$\Delta M[10^{-9}M_*]$	1.59	3.19	8.60		
AT90g44N1	9000 K	z [km]	-7100	-9300	-10280	$H_{\rm v}$ [km]	778
	4.40	P [dyn/cm^2]	1.0*10^6	2.11*10^6	2.80*10^6	$H_{\rm v}$ [H$_{\rm p}$]	0.242
		$\Delta M[10^{-9}M_*]$	1.33	2.80	3.72		

Table 1: **Lower 'boundary' of HeII→HeIII convection zone.** 1. column: Name of the model, 2. column: Effective temperature and logarithm of surface gravity (cgs units), 3. column: Name of the quantities given in the next three columns (The depth in km below $\tau = 1$, the pressure in dyn/cm^2, and the fractional stellar mass of the matter above this depth, given by $\Delta M/M_* = 4\pi GP/g^2$, 4. column: Depth of the boundary of instability (from the Schwarzschild criterion). It coincides for these models with the lower boundary of positive enthalpy flux, 5. column: Depth, where the mean rms value of the vertical velocity is equal to 100 m/s. The maximum rms value of the vertical velocity is always near to 700 m/s. 6. column: Depth of the bottom of the computational domain, 7, 8. column: Velocity scale height, the result of a linear least square fit to the natural logarithm of the mean rms value of the vertical velocity.

For the model AT85g41N3 the same stellar parameters are used as in Sofia and Chan (1984). The models AT85g44N8 and AT85g44N01 include only the lower instability zone. The other four contain both but have a smaller width. The stable region below the superadiabatic layers in the models AT85g41N3, AT85g44N2, and AT90g44N1 is about one pressure scale height deep. The others have a stable region of nearly two pressure scale heights. However, all convectively stable zones in all models show nonzero velocity fields in contrast to standard MLT. The run of the rms velocity with depth can be approximated to a good degree by an exponential curve at the top and at the bottom of both instability zones as it is expected for linear modes penetrating into a region where they cannot propagate (Fig. 3). For the bottom of the HeII→HeIII convection zone the scale height of this curve is $H_{\rm v} \approx \frac{1}{4}H_{\rm p}$. Extrapolating this value to velocities typical for diffusion processes ($v_{\rm diff} \approx 10^{-3}$ cm/s, Michaud, 1970) shows that the influence even of a weak convection zone can reach several pressure scale heights below its MLT boundary.

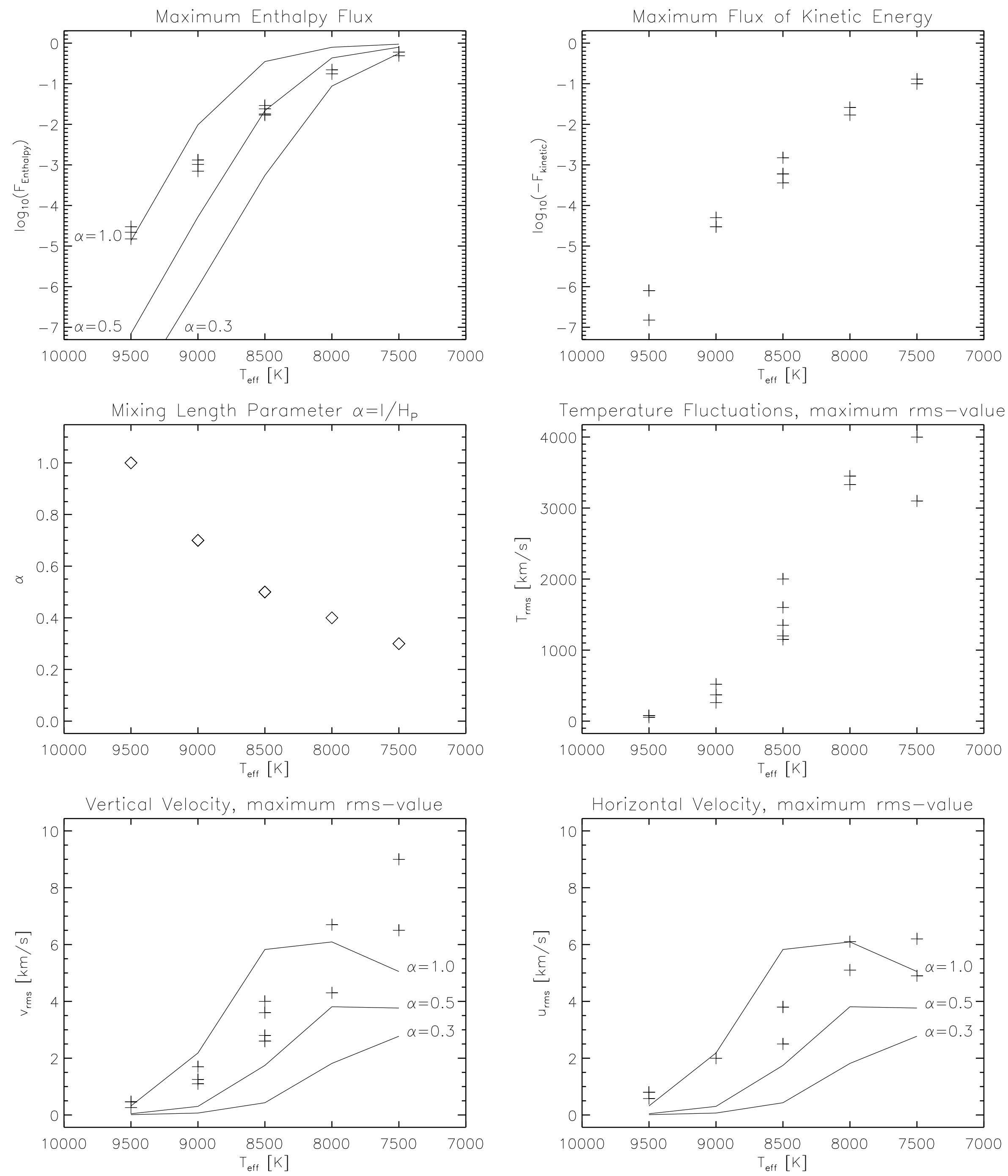

Figure 7: **Data of HD models.** Several quantities characterizing the efficiency of convection are displayed as a function of the effective temperature. Each plus sign indicates a HD model. The scatter at a fixed temperature is due to the effects of different horizontal and vertical extensions, viscosities, grid resolutions, upper boundary conditions, radiation transport (grey or non grey), and versions of the HD code.
Upper left: Plus signs: Maximum value of enthalpy flux $(\max(\overline{F}_{\rm Enthalpy}(z)))$ for different HD models, Solid lines: Maximum value of convective flux for MLT models with different ML parameters $\alpha = l/H_P$, Upper right: Maximum value of kinetic energy flux, Middle left: ML parameter which gives the best fit for the enthalpy flux in the figure above, Middle right: Maximum rms-value of temperature fluctuations, Lower left: Plus signs: Maximum rms-value of vertical velocity, Solid lines: Maximum convective velocity for MLT models with different ML parameters α, Lower right: Plus signs: Maximum rms-value of horizontal velocity, Solid lines: Maximum convective velocity for MLT models with different ML parameters α.

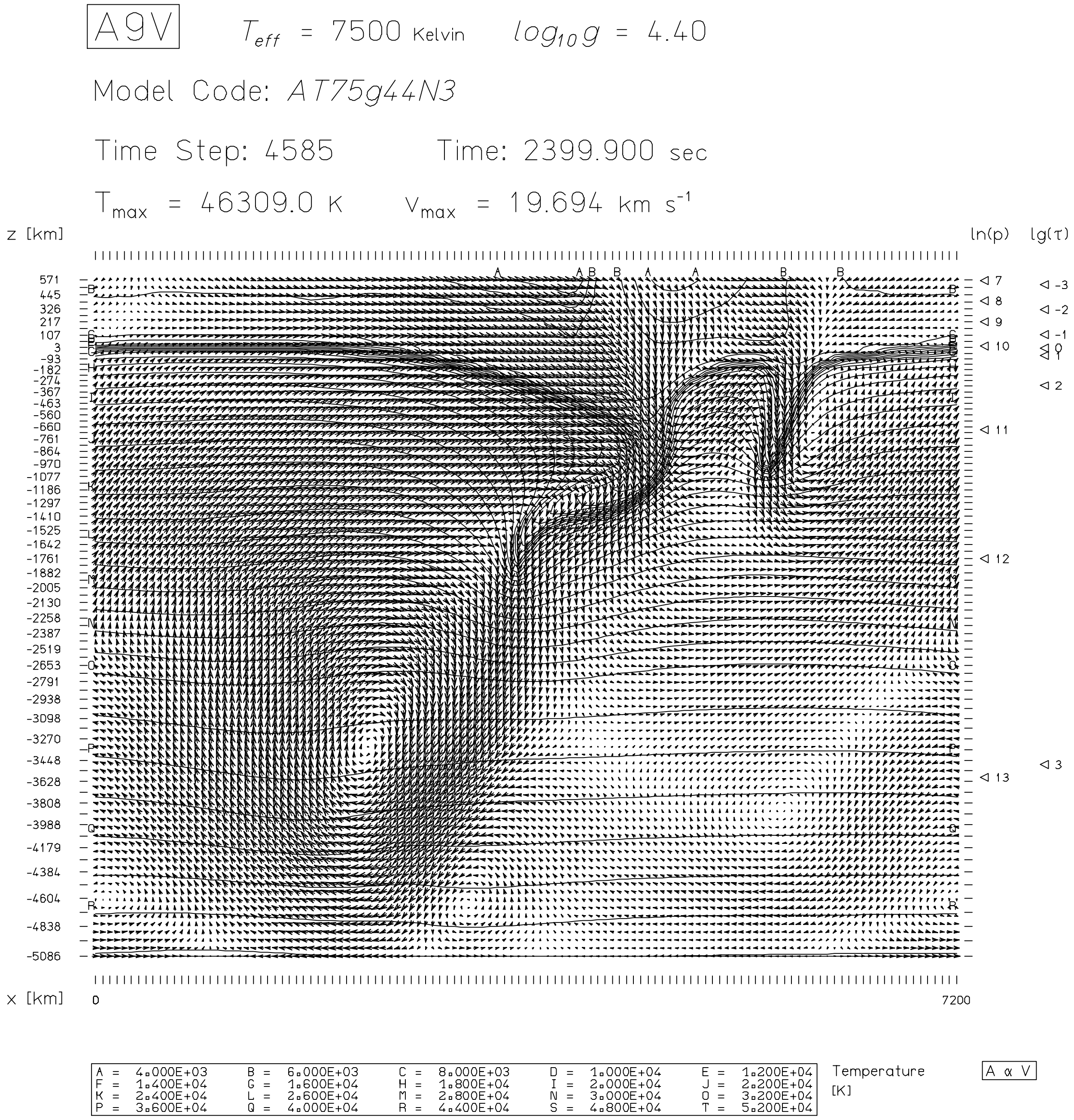

Figure 6: (Model **AT75g44N3**, T_{eff}=7500 K, log$g$=4.40) Snapshot of a typical velocity and temperature field. Temperatures are shown by isotherms in steps of 1000/2000 K, velocities are represented by arrows. The maximum temperature is 46309 K, the highest flow velocity is 19.7 km/s at this instant. In this model convection carries up to 50% of the total flux. The velocity field is extremely violent. The figure shows an instant just before two downdrafts merge which will lead to even larger velocities and to the emission of pressure fluctuations which are radiated into the surrounding medium.

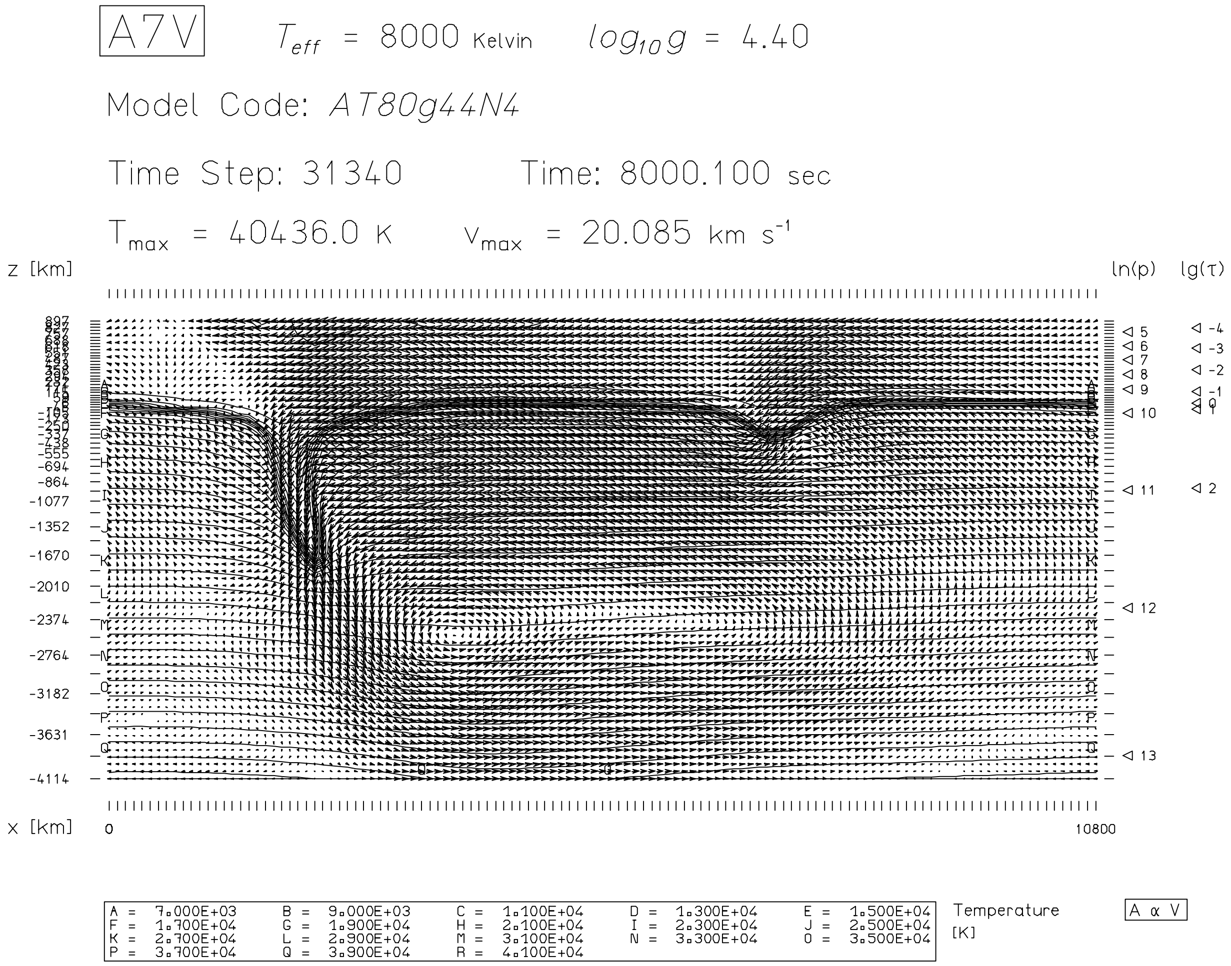

Figure 5: (Model **AT80g44N4**, $T_{\rm eff}$=8000 K, log$g$=4.40) Snapshot of a typical velocity and temperature field. Temperatures are shown by isotherms in steps of 2000 K, velocities are represented by arrows. The maximum temperature is 40436 K, the highest flow velocity is 20.1 km/s at this instant. This model includes only the upper convection zone. Here convection carries up to 20% of the total flux and it cannot be considered as a small disturbance in a stratified medium any more.

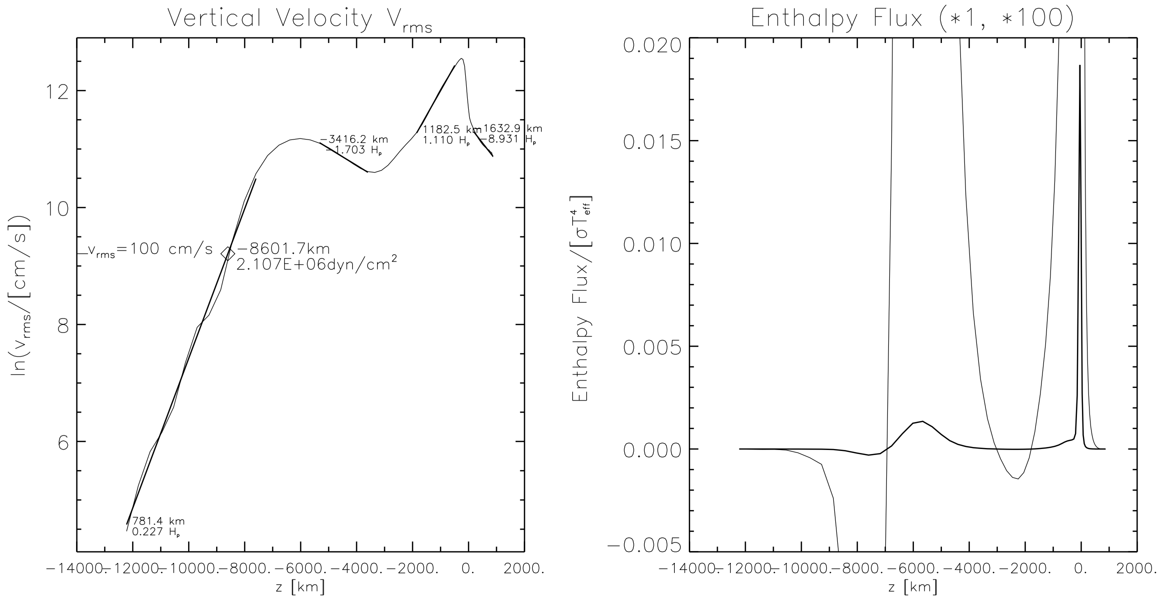

Figure 3: (Model **AT85g44N2**, $T_{\rm eff}$=8500 K, log$g$=4.40) Left: Natural logarithm of rms-value of vertical velocity over height. The velocity scale height is determined by linear least square fits for the four possible cases. It is given in kilometers and pressure scale heights. Right: Mean enthalpy flux over height.
The effects of both partial ionization zones are clearly distinguishable. The HI→HII/HeI→HeII convection zone has higher velocities and a larger enthalpy flux than the HeII→HeIII convection zone.

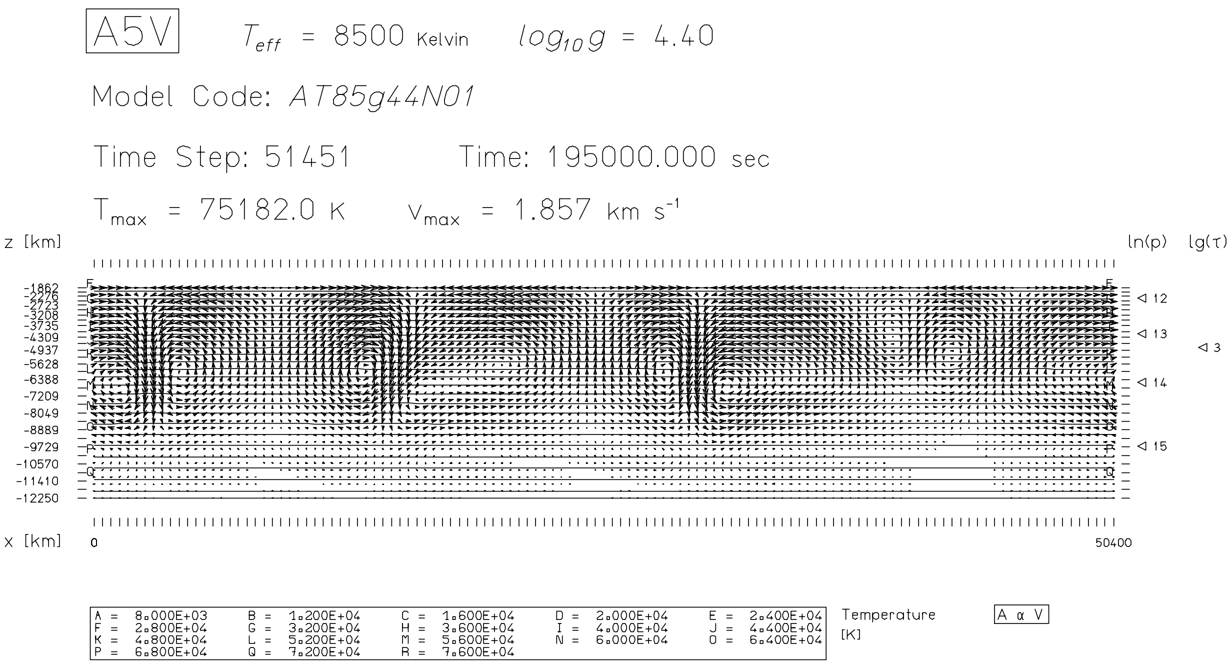

Figure 4: (Model **AT85g44N01**, $T_{\rm eff}$=8500 K, log$g$=4.40) Snapshot of a typical velocity and temperature field. Temperatures are shown by isotherms in steps of 2000 K, velocities are represented by arrows. The maximum temperature is 75182 K, the highest flow velocity is 1.86 km/s at this instant. This model includes only the lower HeII→HeIII convection zone and its upper boundary condition differs from that of the other models. In return its horizontal extension is considerable larger which makes it possible to show more than one single downdraft in this convection zone.

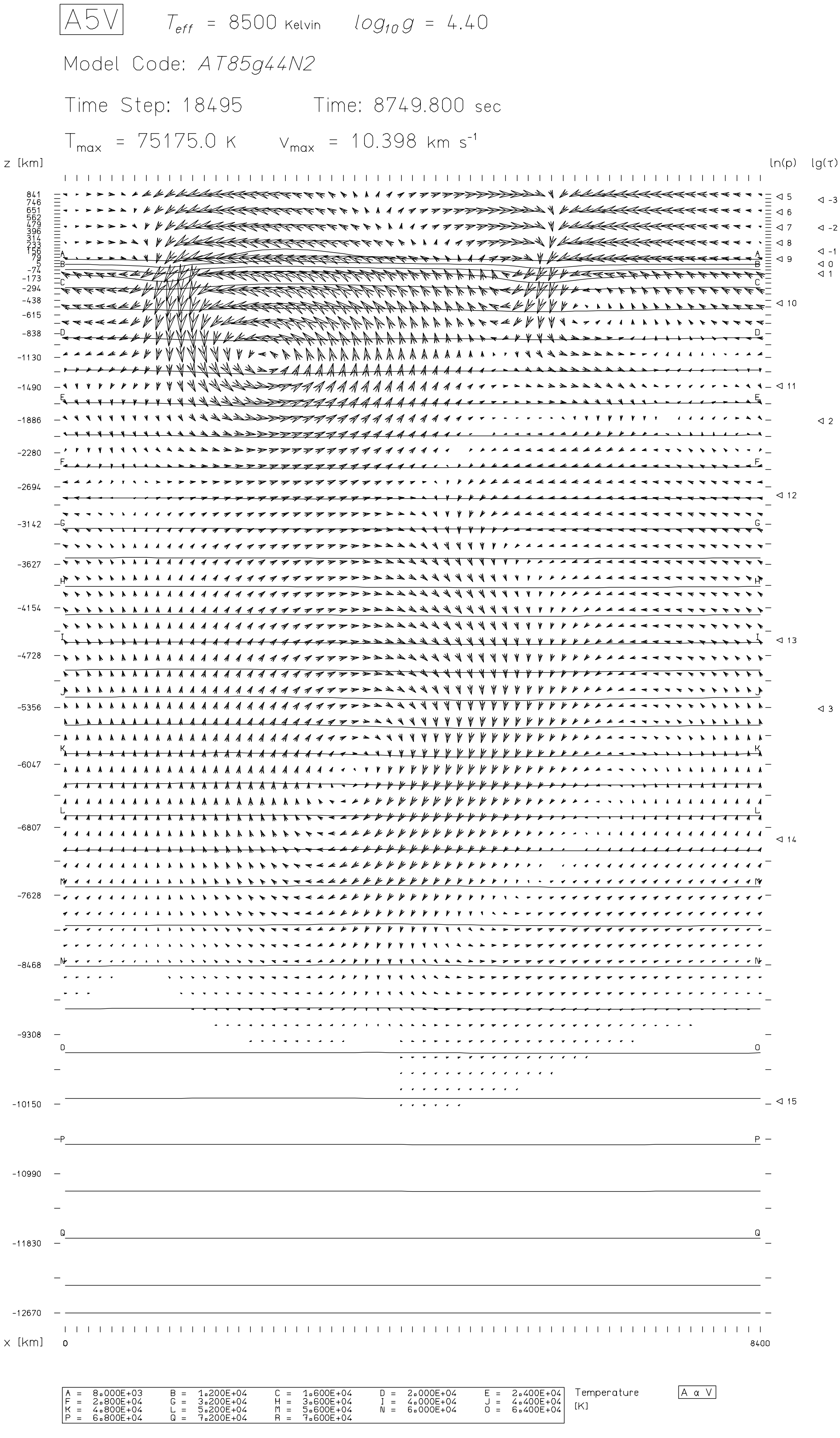

Figure 2: (Model **AT85g44N2**, T_{eff}=8500 K, log$g$=4.40) Snapshot of a typical velocity and temperature field Temperatures are shown by isotherms in steps of 2000 K, velocities are represented by arrows. The maximum temperature is 75175 K, the highest flow velocity is 10.4 km/s at this instant. The velocities, temperature fluctuations and convective fluxes are significantly larger than in the model in Fig. 1. But convection can still be considered as a small disturbance of a plane parallel stratification.

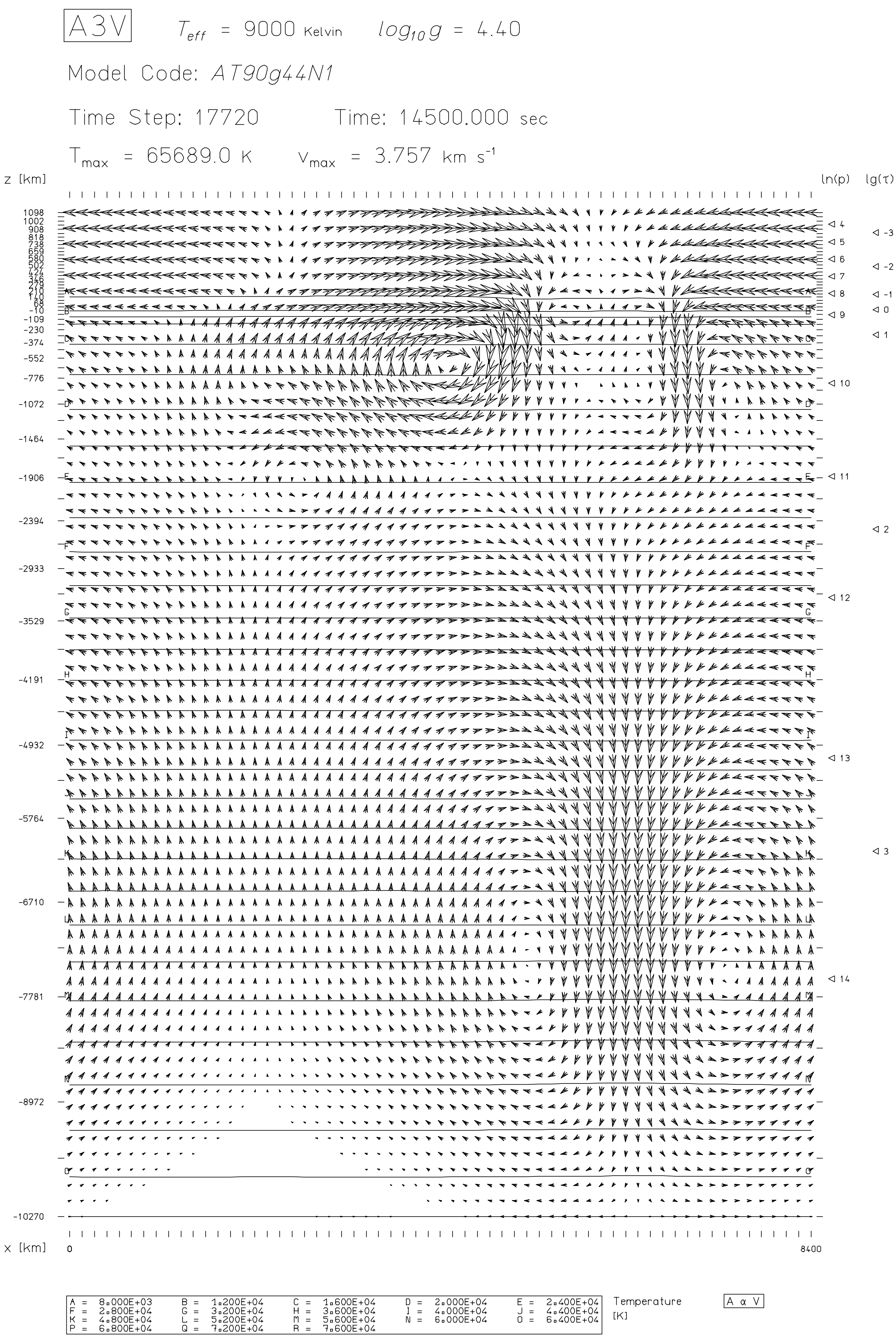

Figure 1: (Model **AT90g44N1**, T_{eff}=9000 K, log$g$=4.40) Snapshot of a typical velocity and temperature field. Temperatures are shown by isotherms in steps of 2000 K, velocities are represented by arrows interpolated to an equidistant grid. Its length is proportional to the square root of the velocity. The maximum temperature is 65689 K, the highest flow velocity is 3.8 km/s at this instant. The velocity corresponding to the smallest arrows is 19 m/s. The calculations are performed on a 62 × 65 grid (indicated by the tic marks at the border of the model) corresponding to a geometrical size of 8400 × 11369 km.
The upper third contains the HI→HII/HeI→HeII convection zone. The lower two thirds contain the HeII→HeIII convection zone. The stratification is nearly plane parallel. Convection carries at most 0.1% of the total flux. However, the computational domain is completely mixed.

tend to merge and form fast deep reaching jets whereas the upstream regions become wider with relatively low velocities. The highest velocities are found in the photosphere as horizontal flows and in the downstream jets.

Strong jets become instationary and start drifting horizontally. They can leave behind quiet regions where due to convective instability new downdrafts can develop (Fig. 5), which again grow, start to move and merge with other jets (Fig. 6). The merging of two jets (= the vanishing of a granule) is a violent event which is accompanied with the generation of pressure fluctuations which are emitted as waves into the surrounding medium.

2 Results

The local MLT model of convection with upward or downward moving bubbles which dissolve after traveling some characteristic length is in strong contradiction to these radiation hydrodynamics simulations. We always find a strong influence of the unstable layers on their convectively stable environment: In the photosphere the velocities may be supersonic and shocks can be found. The region between the H I and the He II ionization region is always completely mixed by overshooting from below and undershooting from above. The lower convection zone has no clearly defined bottom. The velocity field decays in an exponential manner. The velocity scale height is $H_\mathrm{v} \approx \frac{1}{4} H_\mathrm{p}$. So it is possible that the convection mixes ten times more material than it is included in the instability zone, the classical MLT convection zone.

The convective fluxes for different effective temperatures cannot be represented by the same ML parameter α, but it varies from 1.0 to 0.3 for temperatures from 9500 K to 7500 K, respectively.

References

MICHAUD G.: 1970, Diffusion processes in peculiar A stars, *Astroph.J.*, **160**, 641

SOFIAS., CHAN K.L.: 1984, Turbulent Compressible Convection in a deep Atmosphere. II. Two-Dimensional Results for Main-Sequence A5 and F0 Type Envelopes, *Astroph.J.*, **282**, 550

Numerical Simulations of Convection in A Stars

Bernd Freytag
Institut für Theoretische Physik und Sternwarte, Universität Kiel
Olshausenstr. 40, D-24098 Kiel
E-mail: pas24@rz.uni-kiel.d400.de

Abstract

Convective flows in the surface layers of A stars are investigated by means of numerical simulations. These 2-dimensional calculations solve the time-dependent, nonlinear equations of hydrodynamics for a stratified compressible fluid and account for the ionization of H I, He I, and He II and H_2 molecule formation. They include nonlocal, multi-dimensional radiative transfer (grey approximation in LTE).

In contrast to the solar case convection in A stars reaches from the surface only into shallow layers and carries a smaller fraction of the total energy flux. The efficiency of convective energy transport decreases dramatically as the stellar effective temperature increases. The Mixing Length Theory (MLT) predicts a separation of the convection zones due to ionization of H I and He II in hotter A stars.

We determine from our HD models an effective ML parameter α and estimate the depth which is mixed by the convective velocity field.

1 The Models

Models with effective temperatures of 9500 K (extremely weak convection), 9000 K, 8500 K, 8000 K, and 7500 K (efficient convection) with $\log g$=4.40 and different horizontal and vertical extensions were obtained (Fig. 1 to 6). They include the H I partial ionization zone, the He II partial ionization zone, or both. The initial configuration was a grey hydrostatic stratification with small random disturbances in the vertical velocity field in the layers of maximum instability.

During the simulation these disturbances grow and transform into rolls. The up- and downflows are initially symmetric and small scales are favored. This changes when the velocities become larger: The downdrafts